PHILOSOPHICAL TRANSACTIONS A

royalsocietypublishing.org/journal/rsta

Review

Cite this article: Ji H, Goodman J. 2023 Taylor–Couette flow for astrophysical purposes. *Phil. Trans. R. Soc. A* **381**: 20220119. https://doi.org/10.1098/rsta.2022.0119

Received: 31 August 2022
Accepted: 15 December 2022

One contribution of 16 to a theme issue 'Taylor–Couette and related flows on the centennial of Taylor's seminal *Philosophical Transactions* paper (part 2)'.

Subject Areas:
fluid mechanics

Keywords:
Taylor–Couette flow, magnetorotational instability, MHD flow

Author for correspondence:
H. Ji
e-mail: hji@pppl.gov

Taylor–Couette flow for astrophysical purposes

H. Ji[1,2] and J. Goodman[1]

[1]Department of Astrophysical Sciences, Princeton University, Princeton, NJ 08544, USA
[2]Princeton Plasma Physics Laboratory, Princeton University, Princeton, NJ 08543, USA

HJ, 0000-0001-9600-9963

A concise review is given of astrophysically motivated experimental and theoretical research on Taylor–Couette flow. The flows of interest rotate differentially with the inner cylinder faster than the outer, but are linearly stable against Rayleigh's inviscid centrifugal instability. At shear Reynolds numbers as large as 10^6, hydrodynamic flows of this type (quasi-Keplerian) appear to be nonlinearly stable: no turbulence is seen that cannot be attributed to interaction with the axial boundaries, rather than the radial shear itself. Direct numerical simulations agree, although they cannot yet reach such high Reynolds numbers. This result indicates that accretion-disc turbulence is not purely hydrodynamic in origin, at least insofar as it is driven by radial shear. Theory, however, predicts linear magnetohydrodynamic (MHD) instabilities in astrophysical discs: in particular, the standard magnetorotational instability (SMRI). MHD Taylor–Couette experiments aimed at SMRI are challenged by the low magnetic Prandtl numbers of liquid metals. High fluid Reynolds numbers and careful control of the axial boundaries are required. The quest for laboratory SMRI has been rewarded with the discovery of some interesting inductionless cousins of SMRI, and with the recently reported success in demonstrating SMRI itself using conducting axial boundaries. Some outstanding questions and near-future prospects are discussed, especially in connection with astrophysics.

This article is part of the theme issue 'Taylor–Couette and related flows on the centennial of Taylor's seminal *Philosophical Transactions* paper (part 2)'.

THE ROYAL SOCIETY PUBLISHING

royalsocietypublishing.org/journal/rsta Phil. Trans. R. Soc. A 381: 20220119

1. Introduction

Astrophysical interest in Taylor–Couette (hereafter 'TC') flow is motivated by astronomical systems that rotate differentially, usually at extremely large Reynolds numbers. Stars rotate because they form by gravitational contraction from interstellar gas through some 20 orders of magnitude in density, so that any initial vorticity was greatly magnified. Indeed, stars could not form without shedding most of their initial angular momentum, by processes not fully understood [1,2]. While stars are supported against their own gravity mainly by pressure and so are rather round, there is a broad category of very flattened systems called 'discs' whose support is mainly centrifugal. Spiral galaxies belong here, as do the protoplanetary discs recently imaged by the Atacama Large Millimeter Array [3]. Discs around compact objects (white dwarfs, neutron stars and black holes) are usually too compact to be imaged; their rotational flattening is inferred indirectly.

The mass of the disc is usually small compared to that of its central object, leading to a Keplerian angular velocity profile $\Omega \propto r^{-3/2}$, r being the distance from the rotation axis (cylindrical radius). Galactic masses are more extended, so that $\Omega \propto r^{-1}$. For such rotation laws, the specific angular momentum $r^2\Omega$ increases outward, so that Rayleigh's centrifugal instability does not operate. For this reason, TC flows whose outer cylinder is at rest (or counter-rotates) are of limited astrophysical interest. We use the term *quasi-Keplerian* for all rotation laws in which $\partial\Omega/\partial r$ and $\partial(r^2\Omega)/\partial r$ have opposite signs. For an ideal-Couette fluid rotation profile $\Omega(r) = a + br^{-2}$, this requires $ab > 0$.

Most discs accrete: their inner parts flow gradually inward to join the central object. The inflowing gas must shed angular momentum, transferring it outward through the disc via turbulent torques, or expelling angular momentum in a magnetized wind [4]. Absent centrifugal instability, proposed causes of disc turbulence fall into two main categories: (i) a nonlinear or subcritical hydrodynamic shear-flow instability [5,6] and (ii) a linear or supercritical instability of magnetized flow known as the magnetorotational instability (MRI) [7]. It turns out that both of these candidate mechanisms can be actually studied experimentally in TC flow [8,9].

Viscously driven quasi-Keplerian TC flow requires that both cylinders rotate. Figure 1 illustrates the flow regimes defined by the inner (Ω_1) and outer (Ω_2) rotation rates. Both quasi-Keplerian and cyclonic flows, separated by the solid-body line $\Omega_1 = \Omega_2$, are centrifugally stable. Cyclonic flows with the inner cylinder at rest were originally used in the late nineteenth century by Mallock [10,11] and Couette [12] to measure the viscosity of water. This was followed by Wendt [13] and Taylor [14] in 1930s, and by others in later decades. Other than recently predicted linear instabilities in hydrodynamics [15] and in magnetohydrodynamics (MHD) [16], cyclonic flows are subject to subcritical transition to turbulence when the shear Reynolds number is sufficiently large [13,14,17–19]. Cyclonic flow is rare in astrophysics, excepting star-disc boundaries [20,21].

Centrifugally unstable and quasi-Keplerian flows are separated by the Rayleigh stability line [22] $r_1^2\Omega_1 = r_2^2\Omega_2$. The former, which were investigated first by Mallock [10,11] and then by Taylor [23] in 1923 in great detail, are the subject of most papers in this special issue and will not be covered here. Quasi-Keplerian flows are the main subject of this concise review.

We restrict discussion to large Reynolds numbers, defined by $Re \equiv r_1^2\Omega_1/\nu \gg 1$. For narrow gaps ($r_2 - r_1 \ll r_1$), a better definition might be one explicitly based on shear. For example, with the ideal-Couette profile, we might prefer $Re' \equiv b/\nu = \nu^{-1}(\Omega_1 - \Omega_2)/(r_1^{-2} - r_2^{-2})$. This is nearly the same as Re when r_1/r_2 and Ω_2/Ω_1 are significantly less than unity.

The rest of this mini-review will first focus on hydrodynamic experiments in water, and then on MHD using liquid metals. Astrophysical implications of these experiments will be discussed including their future prospects. We conclude with brief citing of TC experiments with stratification, as well as those using gas or plasma.

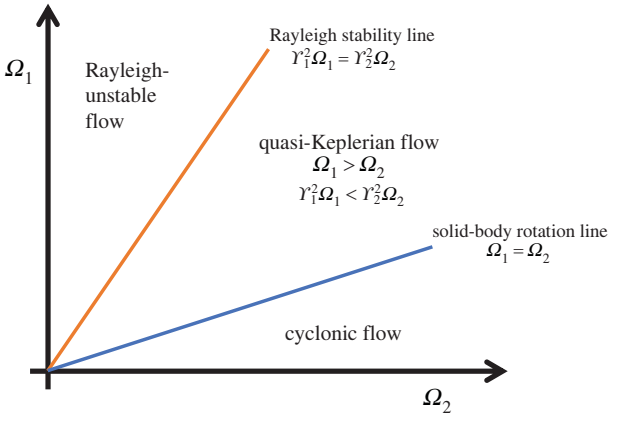

Figure 1. Different Taylor–Couette (TC) flows in the plane (Ω_1, Ω_2) of the rotation rates of the inner (1) and outer (2) cylinders. (r_1, r_2) are the cylinders' radii. (Online version in colour.)

2. Hydrodynamic experiments

The first connection between laboratory TC and accretion-disc flows was made by Zeldovich [5] in 1981 and was followed by Richard & Zahn [6] in 1999, and both were based on subcritical transition to turbulence observed in the cyclonic flows [12–14]. The idea is that, Keplerian flows with sufficiently large Reynolds numbers (as in astrophysics) should always be turbulent due to subcritical transitions despite linear stability, as in cyclonic flows and many other flows. In fact, to our knowledge there have been no exceptions to this hypothesis other than quasi-Keplerian flows (see below).

A contentious debate broke out as to quasi-Keplerian flows are indeed nonlinearly or subcritically unstable to finite-amplitude perturbations, and, if so, how efficiently this mechanism transports angular momentum radially outward. Following the initial suggestions [5,6], many efforts were made and published to study this possibility. None were conclusive, but many authors tended to favour the idea of nonlinear instability, although there were some sceptical astrophysical theorists [18,24,25]. Testing this idea in actual TC experiments in the quasi-Keplerian regime, therefore, became a critical next step, which was performed by several groups in the following years and sometimes accompanied by relevant direct numerical simulations. All relevant experimental and numerical work to date is summarized in table 1.

In the early years of TC flow research, the only documented experiments in the quasi-Keplerian regime were performed by Wendt [13], in the final stages of a scan over Ω_1/Ω_2 starting from the centrifugally unstable regime. The torque data were re-plotted by Coles [38] in his fig. 1, but with no signs of turbulence reported. After a 68-year hiatus, in 2001, the first research devoted specifically to TC flows in quasi-Keplerian regime was published in the PhD thesis of Richard [8]. Richard observed quasi-Keplerian turbulence via Kalliroscope particles and laser Doppler velocimetry, but he did not identify hysteresis in the transitions between laminar and turbulent states, such as he himself confirmed for nonlinear instability in cyclonic flows.

A particular challenge for quasi-Keplerian TC studies is to minimize the effects of the axial boundaries, which would be stress-free in an astrophysical disc. In principle one would have a very large aspect ratio $\Gamma \equiv h/(r_2 - r_1) \gg 1$, but this becomes impractical when one needs a very large Re based on the gap width $r_2 - r_1$. The importance of endcaps was recognized from the beginning when Mallock [11] used mercury as the bottom endcap in an attempt to reduce its effects (the top was a free surface). Endcaps co-rotating with the inner (outer) cylinder induce secondary Ekman circulation that flows radially outward (inward) near the endcaps, with the return flow in the bulk, as shown in figure 2*a*,*b*. This circulation causes the primary azimuthal flow to deviate from the ideal-Couette profile, and vertical shear at the endcaps can produce

Table 1. Experiments and modelling of hydrodynamic TC flow in quasi-Keplerian regimes.

year	author(s)	main results in the quasi-Keplerian regime	method
1933	Wendt [13]	limited measurements of velocity profile and torque; no turbulence reported	Exp
2001	Richard [8]	measured velocity profile affected by endcaps; turbulence identified by flow visualization	Exp
2002	Beckley [26]	measured torque consistent with theoretical predictions for laminar Ekman circulation	Exp
2004	Kageyama *et al.* [27]	measured velocity profile and spin-down time consistent with laminar Ekman circulation	Exp and modelling
2006	Ji *et al.* [28]; Schartman *et al.* [29]	no signs of turbulence at $Re = 2 \times 10^6$ with differentially rotating segmented endcaps	Exp
2008	Obabko *et al.* [30]	confirmed reduction of Ekman cells via segmented endcaps	modelling
2011	Paoletti *et al.* [31,32]	measured enhancement of torque over laminar flow; endcaps attached to outer cylinder	Exp
2012	Avila [33]	up to $Re \approx 6.4 \times 10^3$; bulk flow turbulence driven by segmented endcap rings	modelling
2014	Edlund & Ji [34]	no turbulence despite active perturbations; one endcap ring and two radial rims	Exp
2015	Nordsiek *et al.* [35]	enhanced torque due to axial transport of angular momentum to endcaps	Exp
2015	Edlund & Ji [36]	confirmed *Re* self-similarity of the quiescent flow when Ekman circulation is minimized	Exp
2017	Lopez & Avila [37]	up to $Re \approx 5 \times 10^4$; turbulence confined near endcaps, bulk flow laminar	modelling

turbulence at high enough *Re*. To reduce these effects, Taylor used $\Gamma \sim 100$ [14,23], but the end effects still existed, as evidenced by the deviation from the ideal-Couette profiles [40].

Wendt used a 50/50 split-endcap configuration [13], i.e. the inner (outer) half of the endcap was attached to inner (outer) cylinder (see figure 2*c*), but this appeared to be insufficient at $\Gamma = 5 - 25$. Richard's experiment also employed split endcaps [8] at $\Gamma \approx 25$, but apparently the end effects were still significant (see e.g. his fig. 4.2). Therefore, it is unclear whether the observed turbulence was due to Ekman circulation or to the sought-after nonlinear radial-shear instability.

Endcap effects were demonstrated by two subsequent experiments where endcaps were attached to the outer cylinder (figure 2*a*). In [26], the torque between the cylinders in a short TC ($\Gamma = 2$) flow at $Re \sim 4 \times 10^6$ was dominated by laminar Ekman effects on the endcaps rather than by turbulent transport in the bulk flow. Measurements of flow profiles and spin-down times in an even shorter TC flow ($\Gamma \approx 0.9$) were explained by scaled numerical modelling including the Ekman circulation [27].

Based on this improved understanding, segmented endcap designs using multiple rings with independently controllable rotation speeds were explored via simulations [27,41]. The idea is to break up large Ekman cells that span the full radial gap and pervade the bulk flow into a number of smaller Ekman cells localized to the endcaps. Evidently, the larger the number of small cells, the more closely the Ekman effect is confined to the endcaps. A specific design based on two endrings occupying the full radial gap (figure 2*f*) was implemented in the Princeton MRI experiment [9,42], as shown in figure 3*a*. Its effectiveness at eliminating Ekman effects in the bulk flow has been

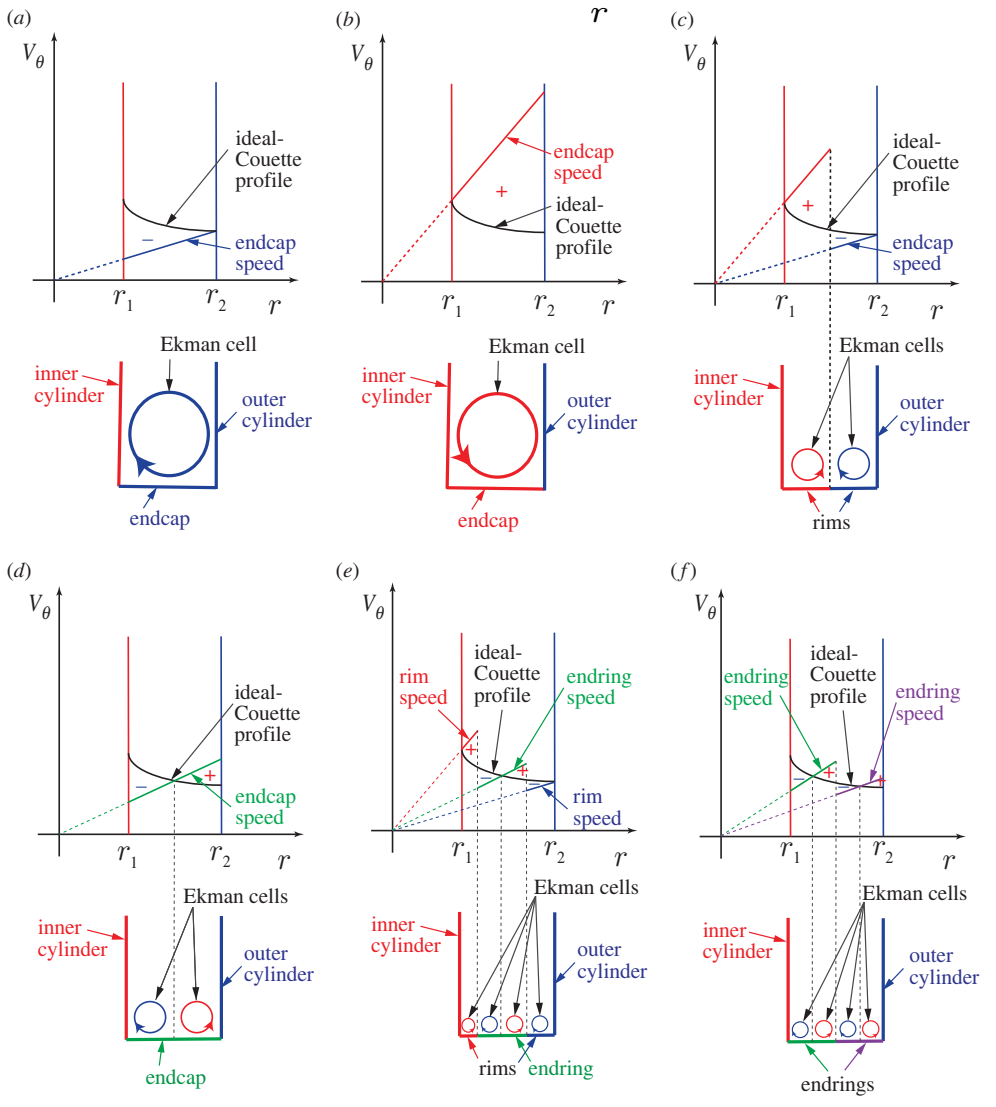

Figure 2. Illustrations of Ekman circulation induced by various endcap configurations. In each panel, the top figure shows colour-coded velocity profiles of the endcaps, endrings or rims. '+' ('−') indicates speeds faster (slower) than the ideal-Couette profile. The bottom figure illustrates counterclockwise Ekman cells in red (clockwise in blue) induced by faster (slower) boundary rotation. (*a*) Endcap (blue) attached to the outer cylinder (OC) [8,13,26,27,31,32,35]; (*b*) endcap (red) attached to the inner cylinder (IC) [13]; (*c*) one rim (red) attached to IC and the other rim (blue) to OC (50/50 configuration [8,13]); (*d*) one ring (green) spanning the radial gap and rotating independently of IC and OC [36]; (*e*) as in (*d*) but with an inner rim (red) attached to IC and the other rim (blue) attached to OC [34,36] and (*f*) segmented endcap design with two independently rotating endrings (green and purple) spanning the radial gap without rims [28,29,39]. (Online version in colour.)

demonstrated by the fact that the ideal-Couette profiles are restored by properly choosing the speeds of two endrings [30,39,43].

A simpler design has been implemented in an experiment at Princeton called HTX (hydrodynamic turbulence experiment) [34]. HTX has a single independently driven endring that is flanked by rims attached to each of the cylinders (figure 2*e*). This is comparably effective to the MRI design at reducing Ekman circulation in the bulk flow, as shown by the azimuthal flow profiles in figure 3*b*. The circulation is divided, and thereby weakened, into the same number

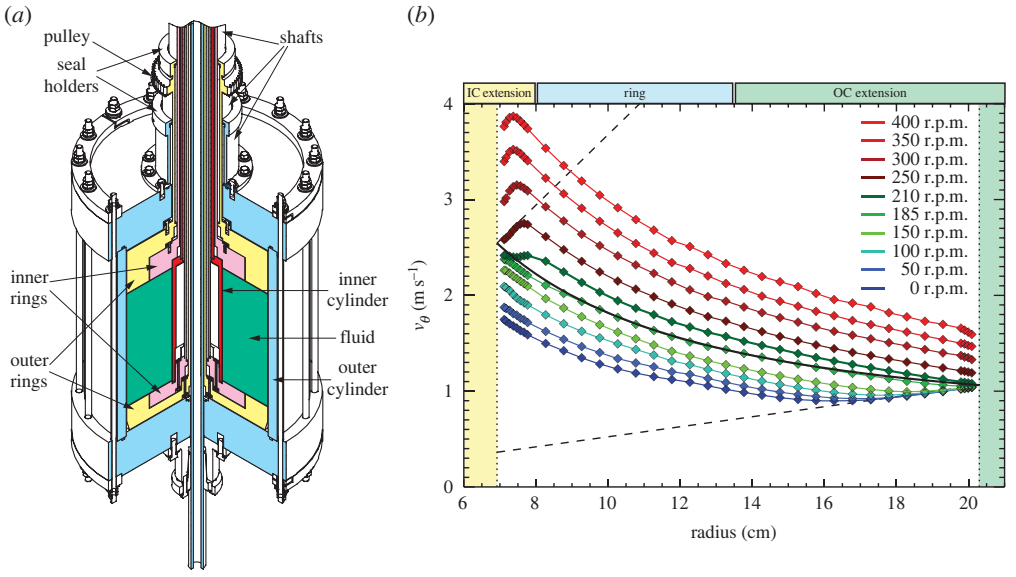

Figure 3. (*a*) Set-up of Princeton MRI experiment during its hydrodynamic phase with two independently rotating endrings and aspect ratio $\Gamma \equiv h/(r_2 - r_1) = 2.1$. Adapted from [28]. (*b*) Measured velocity profiles in HTX ($\Gamma = 2.96$) at various ring speeds; 185 RPM yields a close match to the ideal-Couette profile (solid black line). Adapted from [34]. (Online version in colour.)

of Ekman cells as in the two-ring configuration (figure 2*f*). Various endcap configurations are summarized in figure 2. The key is to increase the number of Ekman cells, while reducing their size, with minimum engineering complexity.

After minimization of Ekman effects, quasi-Keplerian flows are found to be essentially quiescent in the bulk as in solid-body flow, even at shear-based $Re \sim 2 \times 10^6$ [28,29]. Furthermore, the flow reverts promptly to quiescence after perturbations (jets) as large as 20% of the background flow are transiently imposed [34]. This is consistent with numerical simulations for vertically periodic cylinders (hence without Ekman circulation): turbulence decays as soon as the flows enter the quasi-Keplerian regime from the centrifugally unstable one [44], or after an optimal perturbation for transient growth is applied [45].

Reynolds stress and turbulent angular momentum flux have been directly measured by synchronized dual laser Doppler velocimetry, and found to be indistinguishable from zero for optimal endring speeds, at levels comparable to the viscous stress [28,29]. Conversely, with any non-optimal choices of endring speeds or when *Re* is insufficiently large, large Reynolds stresses were detected. These results are also consistent with direct numerical simulations showing that Ekman-driven turbulence penetrates into the bulk flow at low *Re* even with optimal choices of endring speeds [33] while Ekman effects are confined to axial ends at large *Re* [37].

The profound effects of Ekman circulation particularly on quiescent quasi-Keplerian flows offer a plausible explanation of the results reported by Paoletti *et al.* from an experiment at Maryland [31,32]. Significantly larger-than-laminar torques were measured on the middle section of the inner cylinder in an attempt to avoid Ekman effects near the endcaps. However, since the Maryland experiment had an aspect ratios of only $\Gamma = 11.47$ and endcaps attached to the outer cylinder, significant Ekman effects are expected to penetrate well into the bulk flow [33,41]. This was confirmed by velocity profiles measured in the Twente experiment, which had a similar geometry ($\Gamma = 11.68$). These show significant deviation from ideal-Couette profiles over a wide range of parameters in the quasi-Keplerian regime [35]. High-shear flow near the inner cylinder was found to transport angular momentum both radially outward and axially towards endcaps [35].

Although the nonlinear stability of quasi-Keplerian TC flows seems to be settled empirically up to $Re \sim 10^6$, there remain several critical unanswered questions:

- Astrophysical Reynolds numbers are huge: for example, in the so-called minimum-mass solar nebula [46] $Re \equiv |S|h^2/\nu \approx 10^{13}(r/r_\oplus)^{-3/2}$, h being the half thickness of the disc, $r_\oplus \approx 1.5 \times 10^{11}$ m the Earth's orbital radius, and $S = r\mathrm{d}\Omega/\mathrm{d}r = (-3/2)\Omega$ the radial shear. Perhaps quasi-Keplerian flow becomes turbulent at $Re \gg 10^6$ but $<10^{13}$? Experience with subcritically unstable shear flows (e.g. pipe flow [47]) suggests, however, that turbulent momentum transport declines with increasing Re_{crit} when scaled by quantities independent of viscosity. Hence if hydrodynamic disc turbulence exists, it may be feeble.
- Quasi-Keplerian *compressible* plane-Couette flow is linearly unstable when the shear is supersonic [48]. However, instability requires at least one highly reflecting boundary, and peak growth rates are approximately $10^{-3}|S|$ at Keplerian ratios of shear to rotation $(-3/2)$. So the importance of these instabilities for accretion is doubtful, except perhaps in the boundary layer where the disk meets its star [20].
- There can be hydrodynamic disc instabilities driven by vertical (i.e.parallel to the rotation axis) thermal gradients [49]. However, short cooling times are required for rapid growth, and the resulting turbulence tends to be weak and small-scale. More importantly, whether such turbulence can indeed effectively transfer angular momentum *radially*, as demanded in astrophysics, still remains to be seen.
- Can we achieve larger Re experimentally using liquid He or compressed gas?
- Can we achieve larger Re numerically using subgrid models, etc.?
- Most ambitiously, can the nonlinear hydrodynamic stability of quasi-Keplerian flows be proven mathematically? The second and third bullets above suggest that the conditions of any such theorem will need to be carefully formulated.

3. Magnetohydrodynamic experiments using liquid metals

We turn now to TC experiments in which the working fluid is an electrical conductor, usually a liquid metal, and on which a background magnetic field is imposed with axial (B_z) or azimuthal (B_θ) components, or both. Room-temperature liquid metals are rather poor conductors compared to silver, copper or aluminium, so the magnetic diffusivity $\eta = 1/\mu\sigma$, which has the same units as kinematic viscosity, is large and important for such experiments. (Here $\mu \approx \mu_0$ is the magnetic permeability and σ the conductivity of the fluid.) As in hydrodynamics, the flow parameters are best expressed in dimensionless combinations. With η and $B \equiv \sqrt{B_z^2 + B_\theta^2}$, one can form two new independent dimensionless parameters in addition to Re. The magnetic Prandtl number $Pm \equiv \nu/\eta$ is a pure material property, typically 10^{-5} to 10^{-7} in liquid metals. The Lehnert number $Le \equiv V_A/r_1\Omega_1$ compares the Alfvén speed $V_A = B/\sqrt{\mu\rho}$ (the speed of compressionless waves restored by magnetic tension) to the rotation speed, ρ being the fluid mass density. Alternative dimensionless combinations are often used for various ratios of forces or time scales. These include magnetic Reynolds number $Rm = r_1^2\Omega_1/\eta = Pm\,Re$, which compares the time scales of magnetic diffusion and rotation; Lundquist number $Lu = r_1 V_A/\eta = Rm\,Le$; Hartmann number $Ha = r_1 V_A/\sqrt{\nu\eta} = Le\,Re\,Pm^{1/2}$ and Elsasser number $\Lambda = V_A^2/\eta\Omega_1 = Le^2\,Rm$. Since $Pm \lesssim 10^{-5}$, the regime $Rm > 1$, which is necessary for the astrophysically important standard magnetorotational instability (SMRI: see below) can be reached only at $Re \gtrsim 10^5$. However, SMRI has interesting cousins (HMRI, AMRI; also see below) that can be unstable in the limit $Rm \to 0$ provided Ha and Λ are large enough.

The history of SMRI traces back to late 1950s [50,51], but it was not proposed until early 1990s as the source of accretion-disc turbulence [7,52]. The mechanism of SMRI is illustrated by a spring-mass analogue shown in figure 4. The tethered masses exchange angular momentum via tension in the spring. Because of the opposing signs of $\mathrm{d}\Omega/\mathrm{d}r$ and $\mathrm{d}(r^2\Omega)/\mathrm{d}r$, the mass at lower altitude moves ahead in azimuth, progressively losing angular momentum and altitude while increasing its angular velocity; the reverse holds for the other mass. This can be also understood as the

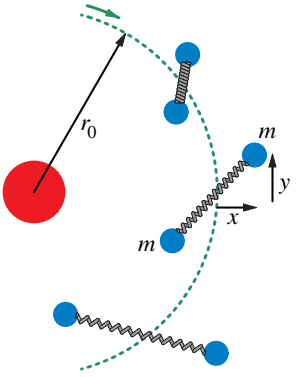

Figure 4. A spring-mass analogue of standard magnetorotational instability (SMRI) originally suggested by A. Toomre (1992, unpublished) and elaborated in terms of a local dispersion relation [53]. Satellites or masses (filled blue circles) of a central gravitating mass (larger filled circle, red) follow near-circular orbits with angular frequencies $\Omega(r)$ while tethered by a weak harmonic spring (grey) having squared natural frequency $\omega_0^2 < -r\mathrm{d}\Omega^2/\mathrm{d}r$. The satellites tend to separate! Conversely, a weak repulsion keeps them together. Adapted from [54]. (Online version in colour.)

increased (decreased) radial force on the inner (outer) mass can overcome the spring force to pull (push) the inner (outer) mass further away from their original positions, leading to a runaway instability. Therefore, this happens only if the spring is sufficiently weak. If the spring is too strong, the perturbations are stabilized (oscillatory).

In SMRI, the role of the spring is played by magnetic tension, exchanging angular momentum between fluid elements on the same field line. In the simple case that the background field is uniform and axial (i.e. parallel to the rotation axis), and in ideal MHD ($\eta = \nu = 0$), the dispersion relation for the complex angular frequency ω reads

$$\omega^4 - \left(2\omega_A^2 + \kappa^2\frac{k_z^2}{k^2}\right)\omega^2 + \omega_A^2\left(\omega_A^2 + r\frac{\mathrm{d}\Omega^2}{\mathrm{d}r}\frac{k_z^2}{k^2}\right) = 0, \tag{3.1}$$

in which $\omega_A^2 \equiv (\boldsymbol{k}\cdot\boldsymbol{V}_A)^2 = k_z^2 B_z^2/\mu\rho$ is in effect the square of the natural frequency of the 'spring,' $k = \sqrt{k_r^2 + k_z^2}$ is the total wavenumber for axisymmetric modes, and $\kappa^2 \equiv r^{-3}\mathrm{d}(r^4\Omega^2)/\mathrm{d}r$ is the square of the epicyclic frequency. Note $\kappa^2 < 0$ and $\omega_A = 0$ yields Rayleigh's centrifugal instability. In the quasi-Keplerian regime, $\kappa^2 > 0$ and $\mathrm{d}\Omega^2/\mathrm{d}r < 0$, instability ($\mathrm{Im}\,\omega > 0$) exists when $0 < \omega_A^2 < -r\,\mathrm{d}\Omega^2/\mathrm{d}r$ so that the last term in equation (3.1) is negative. In non-ideal MHD, with shifted frequencies $\omega_\nu \equiv \omega + i\nu k^2$ and $\omega_\eta \equiv \omega + i\eta k^2$, one has (e.g. [55])

$$(\omega_\nu\omega_\eta - \omega_A^2)^2 + \left[-\kappa^2\omega_\eta^2 + \omega_A^2 r\frac{\mathrm{d}\Omega^2}{\mathrm{d}r}\right]\frac{k_z^2}{k^2} = 0. \tag{3.2}$$

For $\nu > 0$ and $\eta = 0$ ($Pm = \infty$), a marginal mode ($\omega = i0^+$) always exists. But in the opposite limit ($0 \le \nu \ll \eta$), which is relevant for liquid metals, SMRI requires a threshold Rm on the order of unity based on the marginal stability condition $\eta k^2\kappa > (-r\,\mathrm{d}\Omega^2/\mathrm{d}r)/2$ for optimal ω_A^2 and $\kappa^2 > 0$.

Experimentally in TC flows, the spring-mass analogue has been successfully demonstrated [54] using an embedded ball in quasi-Keplerian regime. The ball motion in terms of local Lagrangian displacement x and y (see figure 4 for definitions) follows predictions by the same dispersion relation equation (3.1) when ω_A^2 is replaced by the spring constant and $k_r = 0$ with other minor modifications. Similarly, another analogue of SMRI by viscoelastic instability in polymer fluids where long and elastic polymers act like magnetic field in the linear regime has been verified experimentally [56–58].

By contrast, the search for SMRI in liquid-metal TC flow has been long and arduous, fundamentally because $Pm \ll 1$. This drives one to use wide radial gaps in order to minimize

Table 2. Magnetohydrodynamic TC flow experiments using liquid metal on standard magnetorotational instability (SMRI), helical MRI (HMRI) and azimuthal MRI (AMRI) and relevant direct numerical modelling.

year	author(s)	main results	exp or modelling
2001	Ji *et al.* [9]; Goodman & Ji [42]; Rüdiger & Zhang [59]	proposed realization of SMRI in liquid-metal, quasi-Keplerian TC flow with axial magnetic field	modelling
2004	Sisan *et al.* [60]	claimed detection of SMRI in spherical Couette flow but it turned out to be Shercliff layer instability	Exp
2005	Hollerbach & Rüdiger [61]	predicted HMRI by adding an azimuthal magnetic field with a much reduced critical *Rm*	modelling
2006	Liu *et al.* [62,63]	predicted nonlinear saturation of SMRI	modelling
2006	Liu *et al.* [64,65]	identified HMRI as a weakly destabilized, travelling inertial oscillation, stable in Keplerian flows	modelling
2006	Stefani *et al*. [66,67]	HMRI detected, also with reduced Ekman effects	Exp
2007	Priede *et al.* [68]	inductionless nature of HMRI	modelling
2007	Rüdiger *et al.* [69]; Hollerbach *et al.* [70]	predicted inductionless AMRI with pure azimuthal magnetic field with much lower critical *Rm*	modelling
2009	Boldyrev *et al.* [56]; Bai *et al.* [57,58]	viscoelastic instability in polymer fluids as an SMRI analogue	Exp
2010	Nornberg *et al.* [71]	Shercliff layer instability measured on outer cylinder, interpreted as magnetocoriolis waves	Exp
2011	Gissinger *et al.* [72]	identified the instability observed in spherical Couette flows as Shercliff layer instability	modelling
2012	Roach *et al.* [73,74]; Spence *et al.* [75]	free Stewartson–Shercliff layer instability detected via internal flow measurements and modelling	Exp and modelling
2012	Gissinger *et al.* [76]	imperfect bifurcation to SMRI due to Ekman effects	modelling
2014	Seilmayer *et al.* [77]	AMRI detected	Exp
2016	Wei *et al.* [78]; Winarto *et al.* [79]	effects of conducting endcaps on SMRI: larger amplitude with lower critical *Rm*	modelling
2018	Caspary *et al.* [80]; Choi *et al.* [81]	effects of conducting endcaps on free Shercliff layer instability	Exp and modelling
2019	Hung *et al.* [54]	spring-mass analogue of SMRI in quasi-Keplerian flows	Exp
2021	Vernet *et al.* [82,83]	Keplerian turbulence driven by radial current	Exp
2022	Wang *et al.* [84,85]	first observation of axisymmetric SMRI and a new non-axisymmetric SMRI-like mode	Exp and modelling

ηk_r^2, leading in turn to small aspect ratios and the attendant end effects. Table 2 lists TC flow experiments in liquid metals and relevant direct numerical modelling in quasi-Keplerian regime, including the aforementioned MRI analogues.

The first liquid-metal TC experiment [86] was performed using mercury in the Rayleigh-unstable regime (see figure 1). This was motivated by—and actually confirmed—the theoretical prediction that, contrary to MRI, adding magnetic field stabilizes Rayleigh instability, leading to increased critical *Re* with magnetic field strength [51]. This can be understood from equation (3.2).

Liquid-metal TC experiments attracted limited interest before Balbus & Hawley's theoretical rediscovery of MRI in the early 1990s, and even then only after a proposal to study SMRI in a

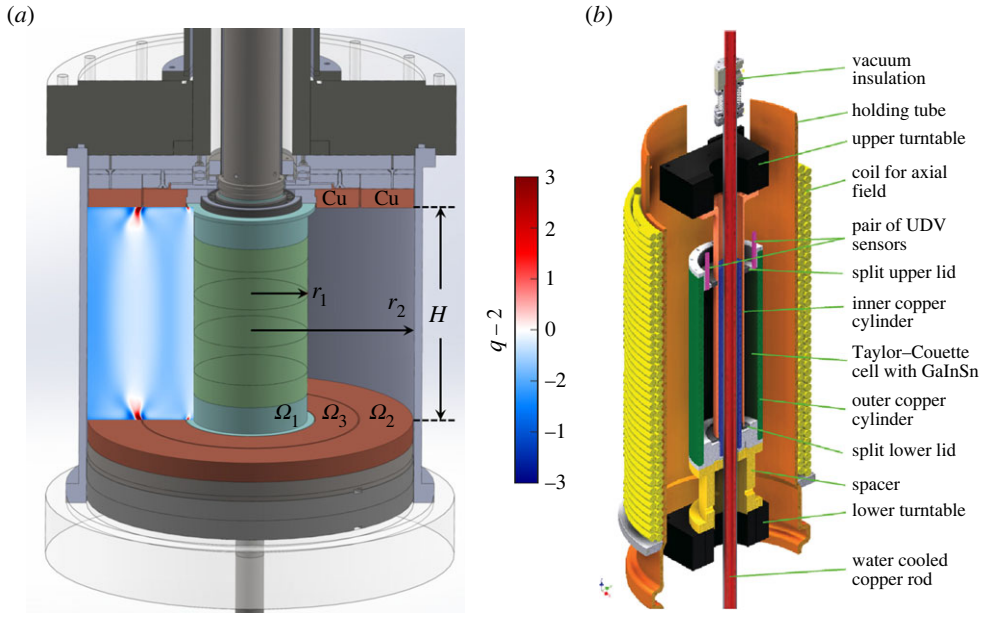

Figure 5. (*a*) The Princeton MRI apparatus with conducting rotating endcaps. Overlaid on the left is the azimuthally averaged shear profile, $q - 2 \equiv -\mathrm{d}\log(r^2\Omega)/\mathrm{d}\log r$, in a 3D hydrodynamic simulation. Adapted from [84]. (*b*) The PROMISE apparatus, supporting both vertical and azimuthal magnetic field. Adapted from [77]. (Online version in colour.)

quasi-Keplerian liquid-gallium TC apparatus [9,42]. The dependence on Pm for such experiments was analysed [59,87], and the feasibility of a liquid-sodium experiment was also shown [88]. Nonlinear saturation [62,63,89,90], and even dynamo action [91] were explored through asymptotic analysis (in narrow gaps, excepting [92]) and numerical simulation. Experimentally, however, SMRI was not positively detected until very recently, another 20 years later [84,85], and only after the proper vertical boundary conditions on endcaps were first studied numerically [78,79], then implemented and confirmed experimentally [80,81].

Endcaps complicate a magnetized liquid-metal TC flow, but can also be exploited to advantage. The complication comes from the enhanced Ekman/Hartmann effects. A discontinuity in the angular velocity at the axial boundary can generate a free Stewartson–Shercliff layer or SSL [93–95] extending vertically into the bulk flow and reinforced by the applied B_z. The layers can be unstable to non-axisymmetric Kelvin–Helmholtz instabilities [71,73–75,80,81]. The magnetized version of SSL instability is inductionless (see below) and occurs when the Elsasser number $\Lambda > 1$. The unstable free SSLs formed tangential to inner sphere of spherical Couette flows [96] also explain [72] a mistaken claim to detect MRI [60].

The advantage of the endcaps in liquid-metal TC experiments comes from the reinforcement of SMRI-unstable rotation via *electrically conducting* endcaps, allowing SMRI to saturate at more detectable amplitudes. In fact, the first attempts to detect SMRI using insulating endcaps failed even though the required rotation speed and magnetic field strength were achieved [74]. This was due to the weak viscous coupling between liquid metal and *insulating* boundaries at $Re \gtrsim 10^6$, so that saturation occurred with undetectably small modifications of the flow and field [89]. To increase the coupling, conducting endcaps using copper were proposed [78], implemented (see figure 5*a* and shown to be effective [80].

However, the magnetically enhanced coupling to the flow via conducting endcaps accentuates the SSL and makes approximating ideal-Couette profiles harder even with segmented endcaps (§2). Radial magnetic field, B_r, the primary diagnostics of SMRI activity, can also be induced by residual Ekman circulation even before the onset of SMRI. Since B_r due to residual Ekman

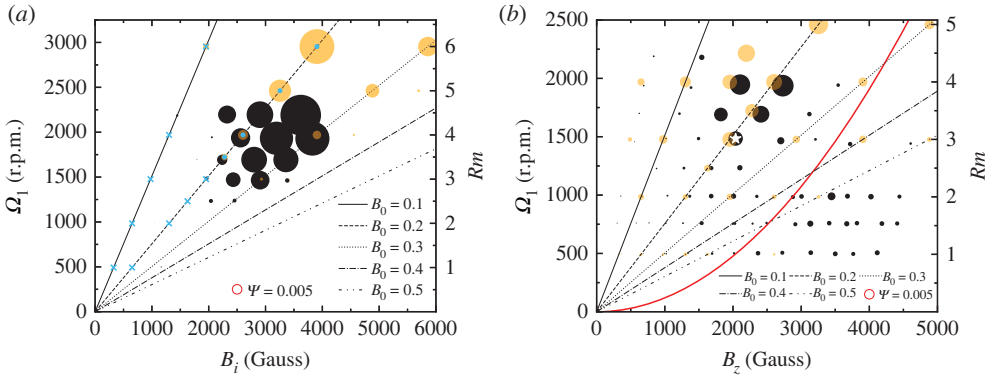

Figure 6. (*a*) 'Bubble plot' of axisymmetric SMRI amplitude from Princeton MRI experiments (black filled circles) and 3D simulations (orange or grey). Bubble diameter is proportional to B_r on the inner cylinder at $z = H/4$, halfway between midplane and upper endcap. Blue crosses and dots show predictions from global linear analysis that the $m = 0$ mode is stable (crosses) or unstable (dots) in a $q < 2$ average bulk profile $\overline{V}_\theta(r)$ from a 3D MHD simulation run to saturation. $B_0 = Le = B_z/r_1\Omega_1\sqrt{\mu\rho}$ is the Lehnert number. Adapted from [84]. (*b*) 'Bubble plot' of $m = 1$ amplitude from experiments (black) and 3D simulations (orange). Bubble diameter is proportional to $m = 1$ radial magnetic field on the inner cylinder at the midplane. Red curve represents the boundary for Stewartson–Shercliff layer instability. Adapted from [85]. Note that the bubble size has been adjusted so that they are on the same scale between two panels. The red circles (marked "Ψ=0.005") show 0.5% of the imposed field. (Online version in colour.)

circulation is proportional to the imposed B_z, the concept of 'imperfect bifurcation' has been introduced [76,97]. Increase of the proportionality B_r/B_z with increasing Rm or Le can be used to identify the SMRI onset [78]. Because of the imperfect bifurcation, the critical Rm is lowered substantially [79] from the linear prediction for ideal-Couette profiles, as an additional benefit of conducting endcaps. An exponential growth phase does not occur because the magnetized flow does not start from a steady state; more precisely, it starts from a hydrodynamic, but not MHD, steady state. Instead, the flow evolves into a new state that is distinctly affected by MRI at large enough Rm. The saturated B_r/B_z amplitude due to SMRI is shown in figure 6*a* in the $\Omega_1 - B_z$ diagram, after removing the contribution from residual Ekman circulation from the measured B_r/B_z. It compares well with data from 3D modelling following the same procedure.

The identified instability exhibits several characteristics of SMRI: unstable only above a critical Rm, and stable when B_z is too small due to finite dissipation and also when B_z is too strong, c.f. the dispersion relations (3.1)–(3.2). The case for SMRI is further supported by global linear analysis of averaged flow profiles over the simulated bulk flow, which is in the quasi-Keplerian regime, i.e. $q < 2$, see figure 5*a*. The B_r/B_z signal becomes large where SMRI is predicted. While these characteristics are consistent with expectations for $m = 0$ SMRI, other explanations cannot be ruled out; further study is called for.

However, there is a surprise. The detected SMRI is axisymmetric (azimuthal mode number $m = 0$), as is predicted to be unstable at the lowest Rm threshold. But in addition, linearly growing non-axisymmetric modes, especially $m = 1$ modes, are also detected [85], and their saturated amplitudes are shown in figure 6*b* in the $\Omega_1 - B_z$ diagram. A subtle but important distinction is that these non-axisymmetric modes are largely *z-independent*, while axisymmetric SMRI modes are *z-dependent* due to their two-cell structure. To place them in their proper prospective, the mode amplitudes are shown in figure 6 based on the same scale, indicating that the $m = 1$ amplitude is at least a factor of 2 less than the $m = 0$ SMRI amplitude measured at $z = H/4$.

These non-axisymmetric mode observations cannot be explained by residual hydrodynamic modes, nor by the SSL instabilities, which exist only to the right of the red curve [85]. They may be related to non-axisymmetric modes found in the narrow-gap limit by Oishi *et al.* [98], but

they occur at Rm smaller by a factor 8–10 than what would be predicted for an ideal-Couette profile. The fact that the $m = 1$ modes are observed in nearly the identical parameter space as the $m = 0$ SMRI modes suggests that they are related. Further study is needed to understand the non-axisymmetric modes. Nevertheless, they have been reproduced numerically in 3D simulations, where they grow exponentially upon the (SMRI-modified) axisymmetric background state, and hence are true linear instabilities [85].

The experimental search for SMRI in liquid-metal TC flows has led to related but inductionless instabilities: helical MRI (HMRI) [61,64,66,67] and azimuthal MRI (AMRI) [70,77,99]. The former involves an imposed field with both azimuthal (B_θ) and axial (B_z) components; the latter, B_θ only. Because of the much lower Re, Ekman effects are important [67]. HMRI is essentially a weakly destabilized $m = 0$ inertial oscillations propagating axially [64], while $m = 1$ AMRI modes propagate azimuthally. Both were first predicted theoretically [61,70] and later confirmed in the PROMISE experiment [66,77] (see figure 5*b*).

Of interest also is a recent novel liquid-metal TC experiment called KEPLER that has a very small aspect ratio, $h \ll r_1, r_2$ [82]. Confined vertically by insulating (Plexiglas) endplates, and radially by stationary conducting cylinders held at different voltages, the azimuthal flow is driven by a radial current and an applied axial magnetic field, a scheme proposed previously to study SMRI [100]. The balance between the applied $\boldsymbol{J} \times \boldsymbol{B}$ force and turbulent drag against the endplates results in a Keplerian profile, $V_\theta \propto r^{-1/2}$. Thus the KEPLER experiment resembles a thin astrophysical disc in its flow profile as well as its geometry. Although the flow transports angular momentum outward [83], the source of its turbulence is probably not any version of MRI, but rather interaction with the endplates.

HMRI, AMRI and the SSL instability are inductionless. By this we mean the magnetic perturbation $\delta\boldsymbol{B}$ can be neglected from the linearized induction equation except where multiplied by the large value η (or Rm^{-1}). It follows that $\delta\boldsymbol{J} = \mu^{-1}\nabla \times \delta\boldsymbol{B} = -(\eta\mu)^{-1}(\boldsymbol{B} \times \delta\boldsymbol{v})_{\rm solenoidal}$, whence the perturbed Lorentz force $\delta\boldsymbol{J} \times \boldsymbol{B}$ becomes $(\eta\mu)^{-1}\,\boldsymbol{B} \times (\boldsymbol{B} \times \delta\boldsymbol{v})_{\rm solenoidal}$. (We are assuming that $\boldsymbol{J} = 0$ in the base state.) Hence the linearized flow does not depend on the background field strength B and diffusivity η independently, but only through combinations that scale as B^2/η. If an inductionless instability exists, then it persists in the limit that $Pm, Rm \to 0$ at fixed Ha ($\propto B/\sqrt{\eta\nu}$) and Λ ($\propto B^2/\eta\Omega$).

Inductionless MHD instabilities are of doubtful relevance to thin astrophysical discs. HMRI requires a larger-than-Keplerian ratio of shear to rotation [64]. More generally, an inductionless instability for which $Rm < 1$ but $\Lambda \gtrsim 1$ will have Lehnert number $Le^2 = B^2/\mu\rho(r\Omega)^2 = \Lambda/Rm > 1$. Yet in thin astrophysical discs, the magnetic energy per unit mass ($B^2/2\mu\rho$) is at most comparable to the thermal energy, which in turn is smaller than the orbital energy $[(r\Omega)^2/2]$ by a factor $\sim (h/r)^2 \ll 1$. Even if Rm is based on the thickness h rather than r, i.e. $Rm \equiv h^2\Omega/\eta$, the magnetic pressure would still have to be larger than the thermal energy.

SMRI is certainly not inductionless: it requires $Rm > 1$ at least. One would like to see the recently reported detections of SMRI [84,85] verified and studied more distinctly at higher Rm, perhaps in the upcoming DRESDYN experiment [101–104] with properly designed axial conducting boundaries despite its favourable large aspect ratio.

4. Conclusion

Over a long history of more than 130 years, quasi-Keplerian Taylor–Couette flow received scant attention until prompted by astrophysical interest about two decades ago. Substantial progress has since been made. In hydrodynamics, the flow is extremely sensitive to axial boundaries. When proper care is taken to minimize Ekman effects, e.g. by using segmented, independently driven endrings, essentially laminar flow prevails at shear Reynolds numbers as large as $Re \approx 10^6$. This is remarkable, as few other shear flows are known to be so stable, and has already suggested applications [105]. It remains to be seen if stability persists to even higher Re, but the results already cast serious doubt on purely hydrodynamic accretion-disc turbulence at least in the unstratified and incompressible limit.

In MHD, SSL instabilities have generated some confusion. Careful endcap design has provided opportunities not only to increase SMRI amplitudes, however, but also to lower threshold magnetic Reynolds numbers $Rm = Pm\,Re$ via imperfect bifurcations. Both developments have facilitated recently reported detections of SMRI, three decades after its astrophysical importance was first recognized. The experimental exploration of nonlinear MRI is a promising field that is only beginning.

Other astrophysically motivated Taylor–Couette work exists that is not covered by this mini-review. This includes stratorotational instability [106, and references therein], which may be relevant to accretion discs with vertical thermal gradients and attendant vertical shear. There is also work on TC experiments with plasma, where flow is driven by biasing electrodes across multipolar edge-mounted magnetic fields [107], or by radial voltages and currents across axial magnetic field [108]. A swirling partially ionized gas experiment in a cylindrical geometry using an injection-pumping system and spiral antennas mounted on endcaps to transmit RF power for plasma production can be used to study SMRI with Hall effects and ambipolar diffusion [109,110]. The tensorial versions of Ohms' Law in these plasma MRI experiments may be relevant to weakly ionized protoplanetary discs [49].

Data accessibility. This article has no additional data.

Authors' contributions. H.J.: writing—original draft, writing—review and editing; J.G.: writing—original draft, writing—review and editing.

All authors gave final approval for publication and agreed to be held accountable for the work performed therein.

Conflict of interest declaration. We declare we have no competing interests.

Funding. Authors acknowledge support by the US Department of Energy via contract no. DE-AC0209CH11466 and National Science Foundation via grant no. AST-2108871.

Acknowledgements. Authors acknowledge assistance by Dr Yin Wang for reformatting figure 6. H.J. thanks the Isaac Newton Institute for Mathematical Sciences, Cambridge, for support during the programme DYT2 (via EPSRC grant no. EP/R014604/1) where some work on this paper was undertaken.

References

1. Mestel L, Spitzer LJ. 1956 Star formation in magnetic dust clouds. *Mon. Not. R. Astron. Soc.* **116**, 503–514. (doi:10.1093/mnras/116.5.503)
2. Zhao B *et al.* 2020 Formation and evolution of disks around young stellar objects. *Space Sci. Rev.* **216**, 43. (doi:10.1007/s11214-020-00664-z)
3. Andrews SM *et al.* 2018 The disk substructures at high angular resolution project (DSHARP). I. Motivation, sample, calibration, and overview. *Astrophys. J. Lett.* **869**, L41. (doi:10.3847/2041-8213/aaf741)
4. Frank J, King A, Raine D. 2002 *Accretion power in astrophysics*. Cambridge, UK: Cambridge University Press.
5. Zeldovich Y. 1981 On the friction of fluids between rotating cylinders. *Proc. R. Soc. Lond. A* **374**, 299–312. (doi:10.1098/rspa.1981.0024)
6. Richard D, Zahn JP. 1999 Turbulence in differentially rotating flows: what can be learned from the Couette-Taylor experiment. *Astron. Astrophys.* **347**, 734–738.
7. Balbus S, Hawley J. 1991 A powerful local shear instability in weakly magnetized disks. I—linear analysis. *Astrophys. J.* **376**, 214–222. (doi:10.1086/170270)
8. Richard D. 2021 Instabilités hydrodynamiques dans les ecoulements en rotation différentielle. Ph.D. thesis, Université Paris 7.
9. Ji H, Goodman J, Kageyama A. 2001 Magnetorotational instability in a rotating liquid metal annulus. *Mon. Not. R. Astron. Soc.* **325**, L1–L5. (doi:10.1046/j.1365-8711.2001.04647.x)
10. Mallock A. 1889 Determination of the viscosity of water. *Proc. R. Soc. Lond.* **45**, 126–132. (doi:10.1098/rspl.1888.0081)
11. Mallock A. 1896 Experiments on fluid viscosity. *Phil. Trans. R. Soc. Lond. A* **187**, 41–56. (doi:10.1098/rsta.1896.0003)
12. Couette M. 1890 Études sur le frottement des liquides. *Ann. Chim. Phys.* **6**, 433–510.

13. Wendt F. 1933 Turbulente Strömungen zwischen zwei rotierenden konaxialen Zylindern. *Ing. Arch.* **4**, 577–595. (doi:10.1007/BF02084936)
14. Taylor G. 1936 Fluid friction between rotating cylinders. I. Torque measurements. *Proc. R. Soc. Lond. A* **157**, 546–578. (doi:10.1098/rspa.1936.0215)
15. Deguchi K. 2017 Linear instability in Rayleigh-stable Taylor–Couette flow. *Phys. Rev. E* **95**, 021102. (doi:10.1103/PhysRevE.95.021102)
16. Mamatsashvili G, Stefani F, Hollerbach R, Rüdiger G. 2019 Two types of axisymmetric helical magnetorotational instability in rotating flows with positive shear. *Phys. Rev. Fluids* **4**, 103905. (doi:10.1103/PhysRevFluids.4.103905)
17. Tillmark N, Alfredsson PH. 1996 Experiments on rotating plane Couette flow. In *Advances in Turbulence VI. Fluid Mechanics and its Applications* (eds S Gavrilakis, L Machiels, PA Monkewitz), vol 36. Dordrecht, The Netherlands: Springer. (doi:10.1007/978-94-009-0297-8_111)
18. Lesur G, Longaretti PY. 2005 On the relevance of subcritical hydrodynamic turbulence to accretion disk transport. *Astron. Astrophys.* **444**, 25–44. (doi:10.1051/0004-6361:20053683)
19. Feldmann D, Borrero-Echeverry D, Burin MJ, Avila K, Avila M. 2023 Routes to turbulence in Taylor–Couette flow. *Phil. Trans. R. Soc. A* **381**, 20220114. (doi:10.1098/rsta.2022.0114)
20. Belyaev MA, Rafikov RR. 2012 Supersonic shear instabilities in astrophysical boundary layers. *Astrophys. J.* **752**, 115. (doi:10.1088/0004-637X/752/2/115)
21. Coleman MSB, Rafikov RR, Philippov AA. 2022 Boundary layers of accretion discs: discovery of vortex-driven modes and other waves. *Mon. Not. R. Astron. Soc.* **509**, 440–462. (doi:10.1093/mnras/stab2962)
22. Rayleigh L. 1916 On the dynamics of rotating fluid. *Proc. R. Soc. Lond. A* **93**, 148–154. (doi:10.1098/rspa.1917.0010)
23. Taylor G. 1923 Stability of a viscous liquid contained between two rotating cylinders. *Phil. Trans. R. Soc. Lond. A* **223**, 289–343. (doi:10.1098/rsta.1923.0008)
24. Balbus SA, Hawley JF, Stone JM. 1996 Nonlinear stability, hydrodynamical turbulence, and transport in disks. *Astrophys. J.* **467**, 76–86. (doi:10.1086/177585)
25. Hawley J, Balbus S, Winters W. 1999 Local hydrodynamic stability of accretion disks. *Astrophys. J.* **518**, 394–404. (doi:10.1086/307282)
26. Beckley H. 2002 Measurements of annular Couette flow stability at the fluid Reynolds Number $Re = 4.4 \times 10^6$: the fluid dynamic precursor to a liquid sodium $\alpha\omega$ dynamo. Ph.D. thesis, New Mexico Institute of Mining and Technology.
27. Kageyama A, Ji H, Goodman J, Chen F, Shoshan E. 2004 Numerical and experimental investigation of circulation in short cylinders. *J. Phys. Soc. Jpn.* **73**, 2424–2437. (doi:10.1143/JPSJ.73.2424)
28. Ji H, Burin M, Schartman E, Goodman J. 2006 Hydrodynamic turbulence cannot transport angular momentum effectively in astrophysical disks. *Nature* **444**, 343–346. (doi:10.1038/nature05323)
29. Schartman E, Ji H, Burin M, Goodman J. 2012 Stability of quasi-Keplerian shear flow in a laboratory experiment. *Astron. Astrophys.* **543**, A94. (doi:10.1051/0004-6361/201016252)
30. Obabko AV, Cattaneo F, Fischer PF. 2008 The influence of horizontal boundaries on Ekman circulation and angular momentum transport in a cylindrical annulus. *Phys. Scr.* **2008**, 014029. (doi:10.1088/0031-8949/2008/T132/014029)
31. Paoletti MS, Lathrop DP. 2011 Angular momentum transport in turbulent flow between independently rotating cylinders. *Phys. Rev. Lett.* **106**, 024501. (doi:10.1103/PhysRevLett.106.024501)
32. Paoletti M, van Gils D, Dubrulle B, Sun C, Lohse D, Lathrop D. 2012 Angular momentum transport and turbulence in laboratory models of Keplerian flows. *Astron. Astrophys.* **547**, A64. (doi:10.1051/0004-6361/201118511)
33. Avila M. 2012 Stability and angular-momentum transport of fluid flows between corotating cylinders. *Phys. Rev. Lett.* **108**, 124501. (doi:10.1103/PhysRevLett.108.124501)
34. Edlund E, Ji H. 2014 Nonlinear stability of laboratory quasi-Keplerian flows. *Phys. Rev. E* **89**, 021004. (doi:10.1103/PhysRevE.89.021004)
35. Nordsiek F, Huisman SG, van der Veen RCA, Sun C, Lohse D, Lathrop DP. 2015 Azimuthal velocity profiles in Rayleigh-stable Taylor–Couette flow and implied axial angular momentum transport. *J. Fluid Mech.* **774**, 342–362. (doi:10.1017/jfm.2015.275)

36. Edlund E, Ji H. 2015 Reynolds number scaling of the influence of boundary layers on the global behavior of laboratory quasi-Keplerian flows. *Phys. Rev. E* **92**, 043005. (doi:10.1103/PhysRevE.92.043005)
37. Lopez JM, Avila M. 2017 Boundary-layer turbulence in experiments on quasi-Keplerian flows. *J. Fluid Mech.* **817**, 21–34. (doi:10.1017/jfm.2017.109)
38. Coles D. 1965 Transition in circular Couette flow. *J. Fluid Mech.* **21**, 385–425. (doi:10.1017/S0022112065000241)
39. Schartman E, Ji H, Burin M. 2009 Development of a Couette-Taylor flow device with active minimization of secondary circulation. *Rev. Sci. Instrum.* **80**, 024501. (doi:10.1063/1.3077942)
40. Taylor G. 1936 Fluid friction between rotating cylinders. II—distribution of velocity between concentric when outer one is rotating and inner one is at rest. *Proc. R. Soc. Lond. A* **157**, 565–578. (doi:10.1098/rspa.1936.0216)
41. Hollerbach R, Fournier A. 2004 End-effects in rapidly rotating cylindrical Taylor–Couette flow. In *AIP Conf. Proc. 733: MHD Couette Flows: Experiments and Models, Acitrozza, Italy, 29 Feb–2 Mar 2004*, pp. 114–121. Melville, NY: AIP Publishing. (doi:10.1063/1.1832141)
42. Goodman J, Ji H. 2002 Magnetorotational instability of dissipative Couette flow. *J. Fluid Mech.* **462**, 365–382. (doi:10.1017/S0022112002008704)
43. Burin MJ, Schartman E, Ji H, Cutler R, Heitzenroeder P, Liu W, Morris L, Raftopolous S. 2006 Reduction of Ekman circulation within a short circular Couette flow. *Exp. Fluids* **40**, 962–966. (doi:10.1007/s00348-006-0132-y)
44. Ostilla-Mónico R, Verzicco R, Grossmann S, Lohse D. 2014 Turbulence decay towards the linearly stable regime of Taylor–Couette flow. *J. Fluid Mech.* **748**, R3. (doi:10.1017/jfm.2014.242)
45. Shi L, Hof B, Rampp M, Avila M. 2017 Hydrodynamic turbulence in quasi-Keplerian rotating flows. *Phys. Fluids* **29**, 044107. (doi:10.1063/1.4981525)
46. Hayashi C. 1981 Structure of the solar nebula, growth and decay of magnetic fields and effects of magnetic and turbulent viscosities on the nebula. *Prog. Theor. Phys. Suppl.* **70**, 35–53. (doi:10.1143/PTPS.70.35)
47. Mullin T. 2011 Experimental studies of transition to turbulence in a pipe. *Annu. Rev. Fluid Mech.* **43**, 1–24. (doi:10.1146/annurev-fluid-122109-160652)
48. Narayan R, Goldreich P, Goodman J. 1987 Physics of modes in a differentially rotating system—analysis of the shearing sheet. *Mon. Not. R. Astron. Soc.* **228**, 1–41. (doi:10.1093/mnras/228.1.1)
49. Lesur G *et al.* 2022 Hydro-, magnetohydro-, and dust-gas dynamics of protoplanetary disks. (https://arxiv.org/abs/2203.09821)
50. Velikhov EP. 1959 Stability of an ideally conducting liquid flowing between cylinders rotating in a magnetic field. *Sov. Phys. JETP* **36**, 995–998.
51. Chandrasekhar S. 1960 The stability of non-dissipative Couette flow in hydromagnetics. *Proc. Natl Acad. Sci. USA* **46**, 253–257. (doi:10.1073/pnas.46.2.253)
52. Balbus S, Hawley J. 1998 Instability, turbulence, and enhanced transport in accretion disks. *Rev. Mod. Phys.* **70**, 1–53. (doi:10.1103/RevModPhys.70.1)
53. Balbus SA, Hawley JF. 1992 Is the Oort A-value a universal growth rate limit for accretion disk shear instabilities? *Astrophys. J.* **392**, 662. (doi:10.1086/171467)
54. Hung DMH, Blackman EG, Caspary KJ, Gilson EP, Ji H. 2019 Experimental confirmation of the standard magnetorotational instability mechanism with a spring-mass analogue. *Commun. Phys.* **2**, 7. (doi:10.1038/s42005-018-0103-7)
55. Pessah ME, Chan CK. 2008 Viscous, resistive magnetorotational modes. *Astrophys. J.* **684**, 498–514. (doi:10.1086/589915)
56. Boldyrev S, Huynh D, Pariev V. 2009 Analog of astrophysical magnetorotational instability in a Couette-Taylor flow of polymer fluids. *Phys. Rev. E* **80**, 066310. (doi:10.1103/PhysRevE.80.066310)
57. Bai Y, Crumeyrolle O, Mutabazi I. 2015 Viscoelastic Taylor–Couette instability as analog of the magnetorotational instability. *Phys. Rev. E* **92**, 031001. (doi:10.1103/PhysRevE.92.031001)
58. Bai Y, Vieu T, Crumeyrolle O, Mutabazi I. 2021 Viscoelastic Taylor–Couette instability in the Keplerian regime. *Geophys. Astrophys. Fluid Dyn.* **115**, 322–344. (doi:10.1080/03091929.2021.1873319)

59. Rüdiger G, Zhang Y. 2001 MHD instability in differentially-rotating cylindric flows. *Astron. Astrophys.* **378**, 302–308. (doi:10.1051/0004-6361:20011214)
60. Sisan DR, Mujica N, Tillotson WA, Huang Y, Dorland W, Hassam AB, Antonsen TM, Lathrop DP. 2004 Experimental observation and characterization of the magnetorotational instability. *Phys. Rev. Lett.* **93**, 114502. (doi:10.1103/PhysRevLett.93.114502)
61. Hollerbach R, Rüdiger G. 2005 New type of magnetorotational instability in cylindrical Taylor–Couette flow. *Phys. Rev. Lett.* **95**, 124501. (doi:10.1103/PhysRevLett.95.124501)
62. Liu W, Goodman J, Ji H. 2006 Simulation of magnetorotational instability in a magnetized Couette flow. *Astrophys. J.* **643**, 306–317. (doi:10.1086/501495)
63. Liu W. 2008 Numerical study of the magnetorotational instability in the Princeton MRI experiment. *Astrophys. J.* **684**, 515–524. (doi:10.1086/590366)
64. Liu W, Goodman J, Herron I, Ji H. 2006 Helical magnetorotational instability in magnetized Taylor–Couette flow. *Phys. Rev. E* **74**, 056302. (doi:10.1103/PhysRevE.74.056302)
65. Liu W, Goodman J, Ji H. 2007 Traveling waves in a magnetized Taylor–Couette flow. *Phys. Rev. E* **76**, 016310. (doi:10.1103/PhysRevE.76.016310)
66. Stefani F, Gundrum T, Gerbeth G, Rüdiger G, Schultz M, Szklarski J, Hollerbach R. 2006 Experimental evidence for magnetorotational instability in a Taylor–Couette flow under the influence of a helical magnetic field. *Phys. Rev. Lett.* **97**, 184502. (doi:10.1103/PhysRevLett.97.184502)
67. Stefani F, Gerbeth G, Gundrum T, Hollerbach R, Priede J, Rüdiger G, Szklarski J. 2009 Helical magnetorotational instability in a Taylor–Couette flow with strongly reduced Ekman pumping. *Phys. Rev. E* **80**, 66303. (doi:10.1103/PhysRevE.80.066303)
68. Priede J, Grants I, Gerbeth G. 2007 Inductionless magnetorotational instability in a Taylor–Couette flow with a helical magnetic field. *Phys. Rev. E* **75**, 047303. (doi:10.1103/PhysRevE.75.047303)
69. Rüdiger G, Hollerbach R, Gellert M, Schultz M. 2007 The azimuthal magnetorotational instability (AMRI). *Astron. Nachr.* **328**, 1158–1161. (doi:10.1002/asna.200710852)
70. Hollerbach R, Teeluck V, Rüdiger G. 2010 Nonaxisymmetric magnetorotational instabilities in cylindrical Taylor–Couette flow. *Phys. Rev. Lett.* **104**, 044502. (doi:10.1103/PhysRevLett.104.044502)
71. Nornberg M, Ji H, Schartman E, Roach A, Goodman J. 2010 Observation of magnetocoriolis waves in a liquid metal Taylor–Couette experiment. *Phys. Rev. Lett.* **104**, 074501. (doi:10.1103/PhysRevLett.104.074501)
72. Gissinger C, Ji H, Goodman J. 2011 Instabilities in magnetized spherical Couette flow. *Phys. Rev. E* **84**, 026308. (doi:10.1103/PhysRevE.84.026308)
73. Roach AH, Spence EJ, Gissinger C, Edlund EM, Sloboda P, Goodman J, Ji H. 2012 Observation of a free-Shercliff-layer instability in cylindrical geometry. *Phys. Rev. Lett.* **108**, 154502. (doi:10.1103/PhysRevLett.108.154502)
74. Roach A. 2013 Velocity measurements and free-shear-layer instabilities in a rotating liquid metal. Ph.D. thesis, Princeton University.
75. Spence EJ, Roach AH, Edlund EM, Sloboda P, Ji H. 2012 Free magnetohydrodynamic shear layers in the presence of rotation and magnetic field. *Phys. Plasmas* **19**, 056502. (doi:10.1063/1.3702006)
76. Gissinger C, Goodman J, Ji H. 2012 The role of boundaries in the magnetorotational instability. *Phys. Fluids* **24**, 074109. (doi:10.1063/1.4737657)
77. Seilmayer M, Galindo V, Gerbeth G, Gundrum T, Stefani F, Gellert M, Rüdiger G, Schultz M, Hollerbach R. 2014 Experimental evidence for nonaxisymmetric magnetorotational instability in a rotating liquid metal exposed to an azimuthal magnetic field. *Phys. Rev. Lett.* **113**, 024505. (doi:10.1103/PhysRevLett.113.024505)
78. Wei X, Ji H, Goodman J, Ebrahimi F, Gilson E, Jenko F, Lackner K. 2016 Numerical simulations of the Princeton magnetorotational instability experiment with conducting axial boundaries. *Phys. Rev. E* **94**, 063107. (doi:10.1103/PhysRevE.94.063107)
79. Winarto HW, Ji H, Goodman J, Ebrahimi F, Gilson EP, Wang Y. 2020 Parameter space mapping of the Princeton magnetorotational instability experiment. *Phys. Rev. E* **102**, 023113. (doi:10.1103/PhysRevE.102.023113)

80. Caspary KJ, Choi D, Ebrahimi F, Gilson EP, Goodman J, Ji H. 2018 Effects of axial boundary conductivity on a free Stewartson-Shercliff layer. *Phys. Rev. E* **97**, 063110. (doi:10.1103/PhysRevE.97.063110)
81. Choi D, Ebrahimi F, Caspary KJ, Gilson EP, Goodman J, Ji H. 2019 Nonaxisymmetric simulations of the Princeton magnetorotational instability experiment with insulating and conducting axial boundaries. *Phys. Rev. E* **100**, 033116. (doi:10.1103/PhysRevE.100.033116)
82. Vernet M, Pereira M, Fauve S, Gissinger C. 2021 Turbulence in electromagnetically driven Keplerian flows. *J. Fluid Mech.* **924**, A29. (doi:10.1017/jfm.2021.635)
83. Vernet M, Fauve S, Gissinger C. 2022 Angular momentum transport by Keplerian turbulence in liquid metals. (https://arxiv.org/abs/2206.14214).
84. Wang Y, Gilson E, Ebrahimi F, Goodman J, Ji H. 2022 Observation of axisymmetric standard magnetorotational instability in the laboratory. *Phys. Rev. Lett.* **129**, 115001. (doi:10.1103/PhysRevLett.129.115001)
85. Wang Y, Gilson E, Ebrahimi F, Goodman J, Caspary K, Winarto H, Ji H. 2022 Identification of a non-axisymmetric mode in laboratory experiments searching for standard magnetorotational instability. *Nat. Commun.* **13**, 4679. (doi:10.1038/s41467-022-32278-0)
86. Donnelly RJ, Ozima M. 1960 Hydromagnetic stability of flow between rotating cylinders. *Phys. Rev. Lett.* **4**, 497–498. (doi:10.1103/PhysRevLett.4.497)
87. Willis AP, Barenghi CF. 2002 Magnetic instability in a sheared azimuthal flow. *Astron. Astrophys.* **388**, 688–691. (doi:10.1051/0004-6361:20020510)
88. Noguchi K, Pariev VI, Colgate SA, Beckley HF, Nordhaus J. 2002 Magnetorotational instability in liquid metal Couette flow. *Astrophys. J.* **575**, 1151–1162. (doi:10.1086/341502)
89. Knobloch E, Julien K. 2005 Saturation of the magnetorotational instability. *Phys. Fluids* **17**, 094106. (doi:10.1063/1.2047592)
90. Umurhan OM, Regev O, Menou K. 2007 Nonlinear saturation of the magnetorotational instability near threshold in a thin-gap Taylor–Couette setup. *Phys. Rev. E* **76**, 036310. (doi:10.1103/PhysRevE.76.036310)
91. Willis AP, Barenghi CF. 2002 A Taylor–Couette dynamo. *Astron. Astrophys.* **393**, 339–343. (doi:10.1051/0004-6361:20021007)
92. Clark SE, Oishi JS. 2017 The weakly nonlinear magnetorotational instability in a global, cylindrical Taylor–Couette flow. *Astrophys. J.* **841**, 2. (doi:10.3847/1538-4357/aa6ff6)
93. Stewartson K. 1957 On almost rigid rotations. *J. Fluid Mech.* **3**, 17–26. (doi:10.1017/S0022112057000452)
94. Shercliff JA. 1953 Steady motion of conducting fluids in pipes under transverse magnetic fields. *Math. Proc. Camb. Philol. Soc.* **49**, 136–144. (doi:10.1017/S0305004100028139)
95. Lehnert B. 1955 An instability of laminar flow of mercury caused by an external magnetic field. *Proc. R. Soc. Lond. A* **233**, 299–302. (doi:10.1098/rspa.1955.0265)
96. Hollerbach R, Skinner S. 2001 Instabilities of magnetically induced shear layers and jets. *Proc. R. Soc. Lond. A* **457**, 785–802. (doi:10.1098/rspa.2000.0692)
97. Knobloch E. 1996 Symmetry and instability in rotating hydrodynamic and magnetohydrodynamic flows. *Phys. Fluids* **8**, 1446–1454. (doi:10.1063/1.868921)
98. Oishi JS, Vasil GM, Baxter M, Swan A, Burns KJ, Lecoanet D, Brown BP. 2020 The magnetorotational instability prefers three dimensions. *Proc. R. Soc. A* **476**, 20190622. (doi:10.1098/rspa.2019.0622)
99. Rüdiger G, Hollerbach R. 2007 Comment on 'Helical magnetorotational instability in magnetized Taylor–Couette flow'. *Phys. Rev. E* **76**, 068301. (doi:10.1103/PhysRevE.76.068301)
100. Velikhov EP, Ivanov AA, Lakhin VP, Serebrennikov KS. 2006 Magneto-rotational instability in differentially rotating liquid metals. *Phys. Lett. A* **356**, 357–365. (doi:10.1016/j.physleta.2006.03.073)
101. Stefani F, Gailitis A, Gerbeth G, Giesecke A, Gundrum T, Rüdiger G, Seilmayer M, Vogt T. 2019 The DRESDYN project: liquid metal experiments on dynamo action and magnetorotational instability. *Geophys. Astrophys. Fluid Dyn.* **113**, 51–70. (doi:10.1080/03091929.2018.1501481)
102. Kirillov ON, Stefani F, Fukumoto Y. 2014 Local instabilities in magnetized rotational flows: a short-wavelength approach. *J. Fluid Mech.* **760**, 591. (doi:10.1017/jfm.2014.614)

103. Mishra A, Mamatsashvili G, Stefani F. 2022 From helical to standard magneto rotational instability: predictions for upcoming liquid sodium experiments. *Phys. Rev. Fluids* **7**, 064802. (doi:10.1103/PhysRevFluids.7.064802)
104. Mishra A, Mamatsashvili G, Stefani F. Submitted. Nonlinear evolution of magnetorotational instability in a magnetized Taylor-Couette flow: scaling properties and relation to upcoming DRESDYN-MRI experiment. (https://arxiv.org/pdf/2211.10811.pdf)
105. Ji H, Cohen A, Efthimion P, Edlund E, Gilson E. 2019 Advanced liquid centrifuge using differentially rotating cylinders and optimized boundary conditions, and methods for the separation of fluids. U.S. Patent Number 10,300,410.
106. Meletti G, Abide S, Viazzo S, Krebs A, Harlander U. 2021 Experiments and long-term high-performance computations on amplitude modulations of strato-rotational flows. *Geophys. Astrophys. Fluid Dyn.* **115**, 297–321. (doi:10.1080/03091929.2020.1795647)
107. Collins C, Katz N, Wallace J, Jara-Almonte J, Reese I, Zweibel E, Forest CB. 2012 Stirring unmagnetized plasma. *Phys. Rev. Lett.* **108**, 115001. (doi:10.1103/PhysRevLett.108.115001)
108. Flanagan K, Milhone J, Egedal J, Endrizzi D, Olson J, Peterson EE, Sassella R, Forest CB. 2020 Weakly magnetized, hall dominated plasma Couette flow. *Phys. Rev. Lett.* **125**, 135001. (doi:10.1103/PhysRevLett.125.135001)
109. Ji H. 2011 Current status and future prospects for laboratory study of angular momentum transport relevant to astrophysical disks. In *Advances in plasma physics: IAU symposium, Giardini Naxos, Italy, Sep 6–10 2010* (eds A Bonanno, E de Gouveia Dal Pino, AG Kosovichev), vol. 274, pp. 18–25. Cambridge, UK: Cambridge University Press.
110. Secunda A, Donnel P, Ji H, Goodman J. Submitted. Magnetorotational instability in a swirling partially ionized gas.